Granular silo flow of inelastic dumbbells: Clogging and its reduction

A. Vamsi Krishna Reddy,[1] Sonu Kumar,[1] K. Anki Reddy,[1] and Julian Talbot[2]
[1]*Department of Chemical Engineering, Indian Institute of Technology Guwahati, Guwahati 781039, India*
[2]*Sorbonne Université, CNRS, Laboratoire de Physique Théorique de la Matière Condensée, LPTMC, F-75005 Paris, France*

(Received 3 April 2018; published 17 August 2018)

We study the discharge of inelastic, two-dimensional dumbbells through an orifice in the bottom wall of a silo using discrete element method (DEM) simulations. As with spherical particles, clogging may occur due to the formation of arches of particles around the orifice. The clogging probability decreases with increasing orifice width in both cases. For a given width, however, the clogging probability is much higher for the nonspherical particles due to their arbitrary orientations and the possibility of geometrical interlocking. We also examine the effect of placing a fixed, circular obstacle above the orifice. The clogging probability depends strongly on the vertical and lateral position of the obstacle, as well as its size. By suitably placing the obstacle the clogging probability can be significantly reduced compared to a system with no obstacle. We attempt to elucidate the clogging reduction mechanism by examining the packing fraction, granular temperature, and velocity distributions of the particles in the vicinity of the orifice.

DOI: 10.1103/PhysRevE.98.022904

I. INTRODUCTION

Clogging is a common, and unwanted, phenomenon during the discharge of a granular material from a silo or hopper. It is also observed in active matter like a herd of sheep passing through a narrow door [1–3], in a crowd of pedestrians [4], panic escape [5,6], and traffic jams [7,8]. Clogging is typically the result of the particles forming an arch in two dimensions [9,10], or a dome in three dimensions [11,12], next to the orifice. Cates *et al.* [13] have termed clogged particles as fragile matter since an entire assemblage can be collapsed by applying a small external force at particular points of the arch. Various methods, including hitting or vibrating the silo [14–16], poking, or aiming compressed air at the arches, have been proposed as practical methods to unclog silos. These solutions, however, have certain limitations in practice. For instance, vibrating a silo may not be economical since it requires energy from an external source.

A recently proposed method to prevent, or reduce, clogging is to place an obstacle above the orifice [2,17,18]. Zuriguel *et al.* [18] have reported that a well-placed obstacle can reduce the clogging probability (CP) by 2 orders of magnitude. They attributed this decrease to the pressure drop in the arch formation region. A similar phenomenon can be observed in active matter. In particular, Zuriguel *et al.* [2] studied the effect of an obstacle on the flow properties of sheep passing through a narrow door. They observed an increase in CP when the obstacle is close to the orifice as temporary clogging occurs between the obstacle and the doorjamb. However, when the obstacle is placed far from the orifice, it does not affect the clogging. Time taken for the egress of sheep was noticed to be minimum at an intermediate position of the obstacle. This suggests the existence of an optimum position to place an obstacle so that clogging will not occur. Recently, the effect of the shape of the obstacle on clogging of spherical particles has been reported [17]. The authors have considered three different shapes of obstacle, namely, circular, triangular, and inverted triangular. They reported that a triangular obstacle is more effective than a circular one in reducing the clogging probability of a system of spherical particles. The effect of height H and diameter D of the obstacle on the dynamics of monodisperse spherical particles discharging out of a silo was analyzed by Lozano *et al.* [19] and that of a hopper by Alonso *et al.* [20].

Most of the 2D and 3D experimental and numerical studies of clogging in silos and hoppers were carried out for systems of spherical particles. However, most granular materials processed in industry, as well as those that occur in natural processes, are aspherical to some degree. Hence, understanding the flow dynamics of nonspherical particules is of great importance. In this regard, Börzsönyi *et al.* [11] conducted 3D experiments to determine the shape effect of granular particles discharging out of a silo using x-ray tomography. They reported that elongated particles prefer to align vertically in the flowing zone. Ashour *et al.* [12] have analyzed the shape and size effect of nonspherical particles on clogging probability, flow rate, and avalanche statistics. Until now, most investigations of nonspherical particulate systems [21–27] have focused on the flowrate. There are few studies that try to understand the physical mechanism above the orifice, where clogging occurs. Moreover, the effect of an obstacle on the flow of nonspherical particulate systems has not yet been investigated, to the best of our knowledge. Therefore, here we present results of 2D numerical simulations of dumbbell-shaped particles discharging from a silo to analyze how the position and size of an obstacle affects the flow dynamics in the region above the orifice. First, we performed numerical simulations in the absence of an obstacle for varying orifice width, W. Then, we placed a circular obstacle of diameter D at various axial, H, and lateral, L, positions while maintaining the orifice width and obstacle diameter constant. Finally, we examined the effect of varying D at fixed H and $L = 0$.

The organization of the paper is as follows. Section II outlines the simulation methodology and the force models

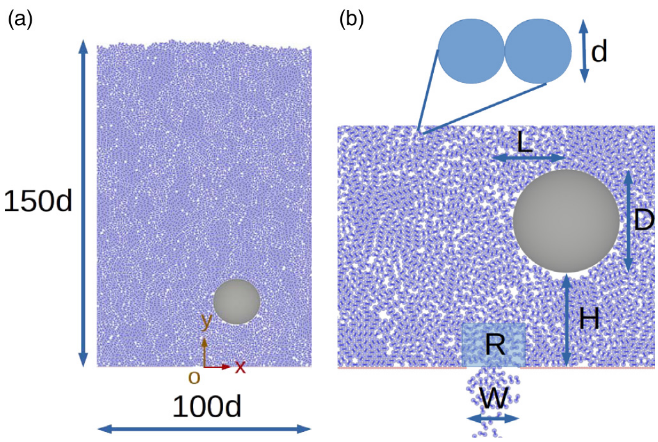

FIG. 1. (a) A configuration from the DEM simulation. (b) View near the orifice. W is the orifice width, H is height of the obstacle, and L is the horizontal distance from axis to the center of the obstacle. The orientation of each dumbbell is indicated by a line joining the centers of the two fused spheres.

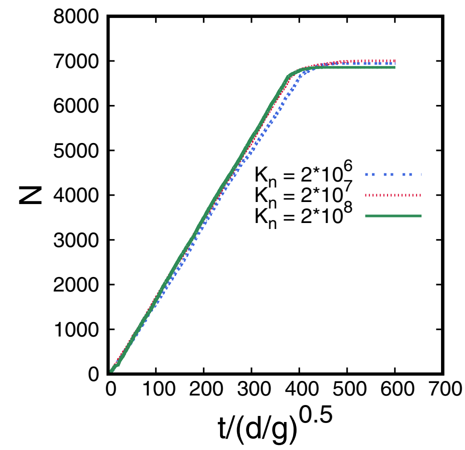

FIG. 2. Number of dumbbells discharged N as a function of time t for different values of the normal elastic constant K_n at $W = 14d$.

used. In Sec. III, results and corresponding interpretations are discussed, and Sec. IV presents our conclusions.

II. SIMULATION METHODOLOGY

We simulated $N = 8000$ dumbbells (a rigid body formed by two fused spheres of diameter d, that means dumbbell's aspect ratio is 2) in a system of size $100d \times 150d$ along x and y, respectively, enclosed by walls at $x = \pm 50d$ and $y = 0$. A gravitational force of magnitude g acts in negative-y direction. The initial configuration is generated by placing particles randomly in space with random orientations and letting them settle in the presence of gravity. This fills the system to a height of roughly $y = 150d$. The system is large enough so that we can neglect any Janssen effect [28]. Figure 1 shows the initial configuration for one of the many cases we have considered in the study. We open the orifice at the beginning of each simulation to allow the discharge of particles in the presence of gravity. The origin is taken as the center of the orifice that is located symmetrically between the two vertical walls.

In our study, we employed the discrete element method (DEM) [29,30] to simulate the gravity-driven flow of dumbbells, essentially a monolayer of dumbbells. We have adopted the contact model suggested by Brilliantov *et al.* [30] to compute the forces between two spheres in contact at a given time. The contact force in the normal direction F^n_{ij} between the particles i and j of radii R_i and R_j, respectively, with an overlap of $\delta_{ij} = R_i + R_j - R_{ij}$, where R_{ij} is the distance between i and j and for the relative velocity (normal direction) of v^n_{ij} is given by $F^n_{ij} = \sqrt{\frac{R_i R_j}{R_i+R_j}}\sqrt{\delta_{ij}}(K_n\delta_{ij}\hat{\boldsymbol{r}}_{\boldsymbol{ij}} - m_{\text{eff}}\gamma_n \boldsymbol{v}^{\boldsymbol{n}}_{\boldsymbol{ij}})$. Here, m_{eff} is the effective mass of the two colliding particles, and K_n and γ_n are the nonlinear spring stiffness and the normal damping coefficient, respectively, in the normal direction. The contact force in the tangential direction F^t_{ij} for a relative velocity (tangential direction) of v^t_{ij} and an overlap of Δs_{ij} and coefficient of friction μ is modelled as follows: $F^t_{ij} = -\min(\sqrt{\frac{R_i R_j}{R_i+R_j}}\sqrt{\delta_{ij}}(K_t \boldsymbol{\Delta s_{ij}} - m_{\text{eff}}\gamma_t \boldsymbol{v}^{\boldsymbol{t}}_{\boldsymbol{ij}}), \mu F^n_{ij})$, where K_t and γ_t are the nonlinear spring constant and the damping coefficient in the tangential direction.

We take $K_n = 2 \times 10^6 \rho d g$ and $K_t = 2.45 \times 10^6 \rho d g$ for a particle of density ρ (mass per unit volume). For a particle of density $\rho = 5000$ kg/m^3 and diameter 20 mm in a gravitational field of $g = 9.8$ m/s^2, this represents roughly a material with a Young's modulus of 1 GPa and Possion's ratio of 0.3 [31]. Moreover, if we take K_n as high as 100 times its current value to represent materials such as steel, the instantaneous flow rate, and number of particles discharged as a function of time barely changes (see Fig. 2). Thus, we can use $K_n = 2 \times 10^6 \rho d g$ to represent realistic materials, at least in the context of the present study.

In our simulations, we choose a damping coefficient $\gamma_n = \gamma_t = 2500\sqrt{g/d^3}$ to represent a realistic coefficient of restitution curve with respect to collision velocity. The coefficient of friction as 0.5 and a time-step of $10^{-4}\sqrt{d/g}$ is chosen in our simulations. The positions and velocities of the dumbbells are defined as the center of mass positions and center of mass velocities of the two adjoining spheres. Forces between the two fused spheres are turned off and by considering the force and torque on the dumbbell as the sum of the forces and torque on each of the constituent spheres. Each simulation is carried out for the time it takes the system to fully discharge or until clogging occurs. The initial configurations are generated independent of each other. All the simulations are carried out using LAMMPS [32] and we used OVITO [33] and VMD [34] for visualization of the simulation trajectories.

III. RESULTS AND DISCUSSION

In this section, we present the main results of our numerical simulations and their interpretation. We have considered four different parameters in our study: the orifice width W, the axial height H, the lateral position L, and diameter D of the obstacle [see Fig. 1(b)]. In Sec. III A, we present the results for the case without any obstacle for varying orifice widths. In Sec. III B, the results for various values of H for $L = 0$ are discussed, while in Sec. III C, the results for various values of L for a fixed

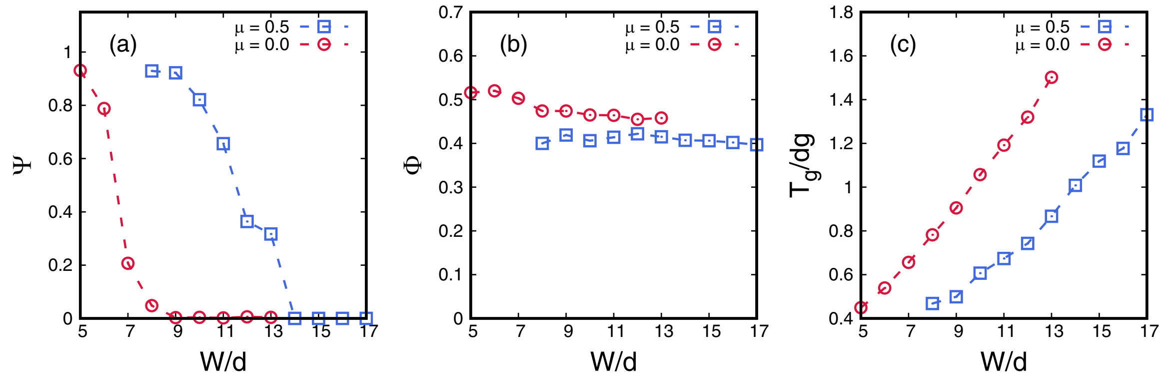

FIG. 3. The variation of (a) clogging index Ψ, (b) packing fraction Φ, and (c) granular temperature T_g with respect to an orifice width of W for a silo without an obstacle.

H are discussed. In Sec. III D, we report results for various values of D for constant H and $L = 0$.

We calculate the clogging index Ψ for a given run i as the ratio of undischarged particles to the initial number of particles. The particles that cannot undergo motion in the silo, such as those in the stagnant zone next to the orifice, are subtracted. The number of particles in the stagnant zone corresponds to the number of undischarged particles when clogging does not happen:

$$\Psi = \frac{1}{n}\sum_{i=1}^{n(\approx 30)} \frac{N_{\mathrm{undis},i} - \overline{N}_u}{N_{\mathrm{total}} - \overline{N}_u}. \qquad (1)$$

Here, $\overline{N}_u = (\overline{N}_{\mathrm{undis},i}) = \sum_i N_{\mathrm{undis},i}/m$, where m is the number of cases in which clogging does not occur, $N_{\mathrm{total}} = 8000$ is the total number of dumbbells in our system, and $N_{\mathrm{undis},i}$ is the total number of particles that remain in the silo before the system's kinetic energy approaches zero for a given run i. Naturally, $N_{\mathrm{undis},i} \approx \overline{N}_u$ for the case of full discharge.

Region R is defined above the orifice as shown in Fig. 1(b) with a length of $(W + 2d)$ along x and $10d$ along y. The packing fraction Φ of the particles in region R is calculated as the ratio of the volume of particles contained within it to the total volume of the region R. Since this system is quasi-two-dimensional, its thickness is taken as d for calculating the volume of region R. The granular temperature is computed for region R as $T_g = \frac{1}{2}\langle (v_x - < v_x >)^2 + (v_y - < v_y >)^2 \rangle$ where $< . >$ denotes the spatiotemporal mean. All the results presented, including the velocity distributions, are averaged over approximately 30 independent runs using different initial configurations. We calculate all the quantities of interest by averaging over time until clogging, or full discharge, occurs. We neglected any run in which clogging occurs before a minimum of 100 dumbbells are discharged from the silo.

A. Without obstacle

In this subsection, clogging of dumbbells in the absence of an obstacle is discussed for various orifice widths W. The discharge of the dumbbells is initiated by opening the orifice at time $t = 0$.

In Fig. 3(a), we show the clogging index Ψ as a function of the orifice width W for frictionless ($\mu = 0.0$) and frictional ($\mu = 0.5$) particles. One observes that the clogging index of frictional particles is almost unity for $W \leqslant 9d$, while it is approximately zero for $W \geqslant 14d$. Börzsönyi *et al.* [11] and Ashour *et al.* [12] performed experiments to understand the flow of shape-anisotropic particles of different aspect ratios in a 3D silo with a circular orifice. They considered the existence of critical orifice radius above which clogging events are improbable and they argue that this critical orifice radius (typically defined as the ratio of orifice radius W_c to the equivalent radius of a spherical particle of volume equal to that of an aspherical particle, l_{eq}) is very high for elongated grains. For disks in two dimensions, this ratio is found to lie between 4 and 5 [35]. In our case, however, we observe that the critical width W_c lies between $13d$ and $14d$ corresponding to a critical ratio in the range $10.3 < W_c/l_{\mathrm{eq}} < 11.1$. This is in contrast to what is observed in the case of circular particles. Even if we consider the longest dimension of the dumbbells $2d$, $W_c/l_{\max}$ comes out to be around 6.5 to 7.0. Moreover, for frictionless dumbbells, critical orifice width lies between $8d$ and $9d$, while it is slightly larger than d for hydrogel particles (practically frictionless) used in Ref. [36]. This high critical width ratio is due to many factors, including an orientational barrier, geometrical interlocking, and a larger surface area of

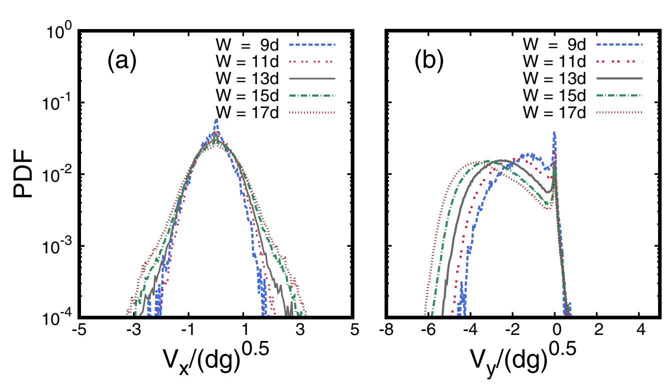

FIG. 4. The probability distribution of (a) velocity component along x and (b) velocity component along y in region R for a silo without an obstacle.

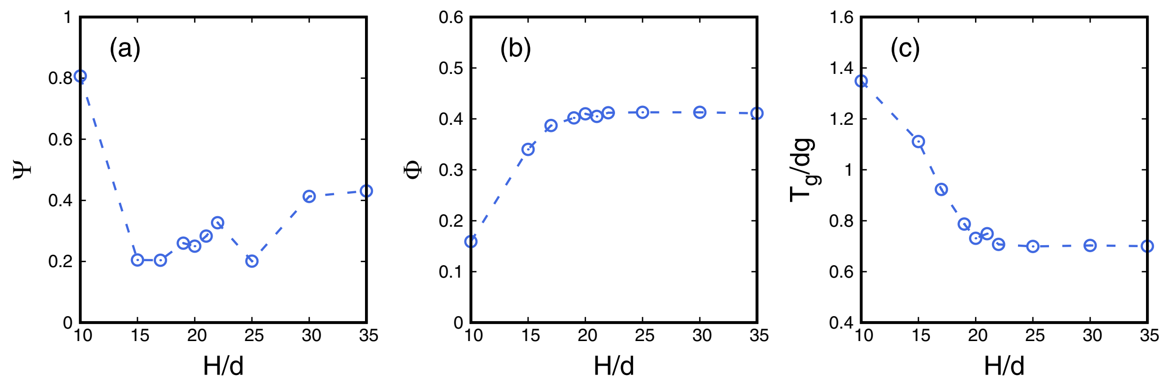

FIG. 5. The variation of (a) clogging index Ψ, (b) packing fraction Φ, (c) granular temperature T_g with respect to the vertical position of obstacle H at $L = 0$, $W = 11d$, and $D = 22d$. All parameters are computed for particles in region R.

interaction compared to spheres. Clogging can be induced due to an improper orientation. An example of this in real life would be attempting to get a couch through a door. If the couch is improperly oriented it will not pass through. Similarly, an aspherical particle will experience the same difficulty. This, in turn, also induces anisotropy in the orientational ordering as seen in Ref. [11]. Geometrical interlocking plays a role not just in enhancing clogging but also in stabilizing the clogged arch that is formed. Spherical particles have the least interlocking of all the particle shapes.

In Figs. 3(b) and 3(c), we plot the packing fraction Φ and the granular temperature T_g (nondimensionalized by dg), respectively, of the dumbbells contained in region R as a function of W. We notice that Φ is almost constant, indicating that Ψ remains independent of Φ in the absence of an obstacle. The granular temperature T_g, however, increases with the orifice width. This can be explained by the increase in fluctuations of the velocity components as W increases, which is due to an increase in the collision rate between the particles when particles on either side of the silo meet at the orifice. This increase in T_g with W can also be explained by plotting the horizontal and vertical velocity distributions, v_x and v_y, respectively, as shown in Fig. 4. The width of the distribution of horizontal and vertical velocity components of particles in region R increases as W is increased.

B. Axial variation of the obstacle position

In the silo flow of spherical particles, Zuriguel *et al.* [18] observed that placing an obstacle at an appropriately chosen height above the orifice can greatly decrease clogging compared to a system with no obstacle. In this subsection we examine how effectively the presence of obstacle ($D = 22d$) can reduce the clogging of dumbbell-like particles while they are flowing through a narrow opening at the bottom of a silo. Here we varied the vertical position of the obstacle H above an orifice of width $W = 11d$. (At this width in the absence of an obstacle, $\Psi = 0.66$, and so we expect the clogging to be sensitive to perturbations induced by the obstacle). In Fig. 5(a), we see that the clogging index is very high when the obstacle is close to the orifice. This is due to the formation of arches between the obstacle and exiting particles. However, we see that when the obstacle is positioned sufficiently far above the exit, the clogging index tends to approach that of the no obstacle case. This is explained by the fact that as the height of the obstacle increases, the more its effect on the flow at the exit diminishes, thus mimicking the no obstacle case. At intermediate heights, however, low values of the clogging index are observed. We see two local minima in Ψ [see Fig. 5(a)] at which $\Psi \approx 0.2$. i.e., about a threefold reduction compared to a silo with no obstacle.

Another intriguing observation is the presence of a maximum at $H = 22.5d$. This behavior is explainable in terms of the type of clogging arch that is formed. We observe that in the presence of an obstacle two types of clogging arches occur, namely one that involves and one that does not involve the obstacle. When the obstacle is very close to the orifice, clogging is mostly due to the first type while when it is far away, the clogging arches are formed only by the particles. Both types of arches are displayed in Fig. 6. When $H = 10d$, only the first type of arch is observed while for $H = 15d$ and $17.5d$ both types are observed. The first decrease

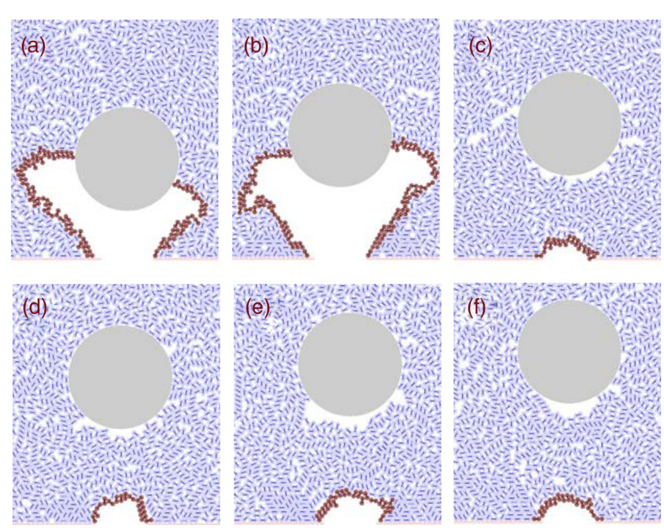

FIG. 6. Clogged states at $H =$ (a) $10d$, (b) $15d$, (c) $17.5d$, (d) $20d$, (e) $22.5d$, and (f) $25d$ with an orifice width of $W = 11d$.

TABLE I. Average width w_{avg} and height h_{avg} and standard deviation of width σ_w and height σ_h of the arches averaged over n clogged states. The first row represents the case without an obstacle, the next set of rows are for a case with an obstacle and the last two rows represent the case of frictionless system without an obstacle.

W or H	w_{avg}	σ_w	h_{avg}	σ_h	n
$W = 11d$	12.43	0.54	8.47	2.22	10
$H = 10d$	12.75	0.76	18.99	4.19	14
$H = 15d$	12.26	1.15	18.08	10.59	10
$H = 17.5d$	11.74	0.68	9.31	8.91	12
$H = 19d$	12.19	1.02	8.47	7.73	10
$H = 20d$	11.84	0.77	6.59	2.23	12
$H = 21d$	11.54	0.75	7.13	2.22	13
$H = 22.5d$	12.23	0.68	7.94	1.95	10
$H = 25d$	12.25	0.9	7.86	3.61	10
$H = 30d$	12.12	0.7	8.13	2.07	15
$H = 35d$	12.04	0.65	6.96	1.5	14
$W = 7d$	8.5	1.33	4.75	2.35	14
$W = 6d$	6.6	0.72	3.81	2.02	10

in the clogging index at $H = 15.0 - 17.5d$ [see Fig. 5(a)] corresponds to the transition from the first type of clogging arch to the second type. For $H \geqslant 20d$, only the second type of arch is observed. This can be explained by the difference in standard deviations in vertical heights of the arches as shown in Table I. The decrease in Ψ at $H = 25d$, which is not observed in the case of spherical particles, could be due to the changes in orientation dynamics of the particles due to the presence of obstacle as shown in Fig. 7. Analyzing the orientation dynamics of anisotropic particles in silo flows, is an important future problem. Figures 5(b) and 5(c) show the variation of Φ and T_g in region R with respect to H of the obstacle. We see that the packing fraction increases gradually while the granular temperature decreases with respect to H and both quantities saturate for $H > 21d$. The presence of an obstacle close to the orifice reduces Φ due to the wake formed below the obstacle. It

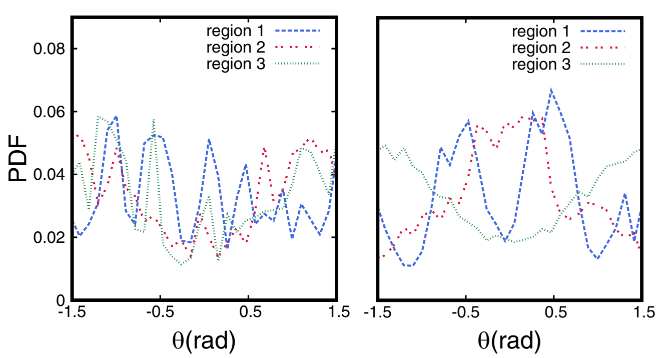

FIG. 7. PDF of orientation angle θ of the dumbbells. θ is defined as the angle between dumbbell axis and x axis. Region 1 is far above the obstacle at $90 < y < 100$, region 2 is just above the obstacle at $40 < y < 50$, and region 3 is above the orifice at $0 < y < 10$. All regions are considered in $-5 < x < 5$. The left side plot is for a silo without an obstacle and right side plot is for a silo with an obstacle at $H = 25d$. Here, $W = 11d$. All the results are averaged over several configurations.

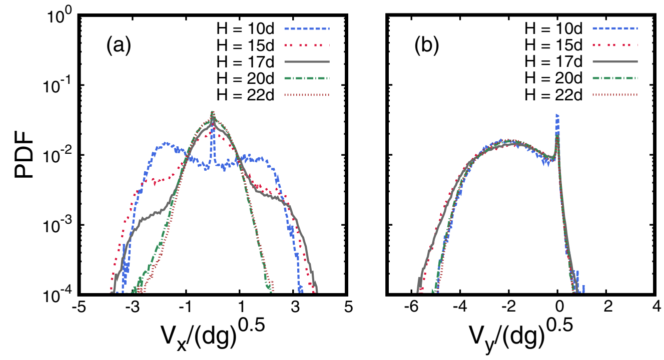

FIG. 8. The probability distribution of the (a) horizontal and (b) vertical velocity component of particles in region R for a silo with $W = 11d$ containing an obstacle of $D = 22d$.

also increases the fluctuation in velocities of particles in region R as the particles moving on the alternate side of the obstacle collide in region R giving rise to high fluctuations. This can be seen in Fig. 8, which shows the distributions of the horizontal and vertical velocity components.

C. Lateral variation of the obstacle position

Earlier studies have shown the existence of optimal location of an obstacle for reducing clogging in the discharge of spherical particles from a silo [17], as well as for sheep passing through a narrow door [2]. In the present work, we examine if a *lateral* displacement of the obstacle leads to the reduction in the clogging. When the obstacle is displaced laterally, particles flowing around the silo interact differently with the stagnant zones present on either side of orifice, and this may lead to a change in the clogging index Ψ.

We observe that displacing the obstacle laterally may reduce clogging. Although the clogging index shown in Fig. 9(a) shows variability it does show that there exists at least one location at which the clogging index Ψ is lower when compared with the case for $L = 0$. Moreover, the presence of an obstacle away from $L = 0$ also increases the packing fraction of the particles in region R up until $L/d \approx 10$ beyond which there is no dependence. The wake formed below the obstacle lies completely inside the region R for $L = 0$ and $H = 10d$. However, for $L \geqslant 5d$, only a part of wake lies in region R thus providing more room for particles to fill.

The granular temperature T_g decreases with L [see Fig. 9(c)]. When an obstacle is located symmetrically, i.e., $L = 0$, then the flow is separated into two halves that collide below the obstacle. However, as we increase L the flow rate on the right side of the obstacle decreases thereby reducing the collision rate as shown in Fig. 10. This could be the reason behind the decrease in granular temperature.

The distribution of the horizontal velocity component at $H = 10d$ is shown in Fig. 11(a). The plot is symmetric and the width of distribution is greater at $L = 0$, since in this position the obstacle forces the particles to flow on either side of the obstacle. However, for $L \geqslant 5d$, the obstacle blocks particles flowing from the right side. Now if we focus on the case of $L = 5d$, even the particles on the right side are forced

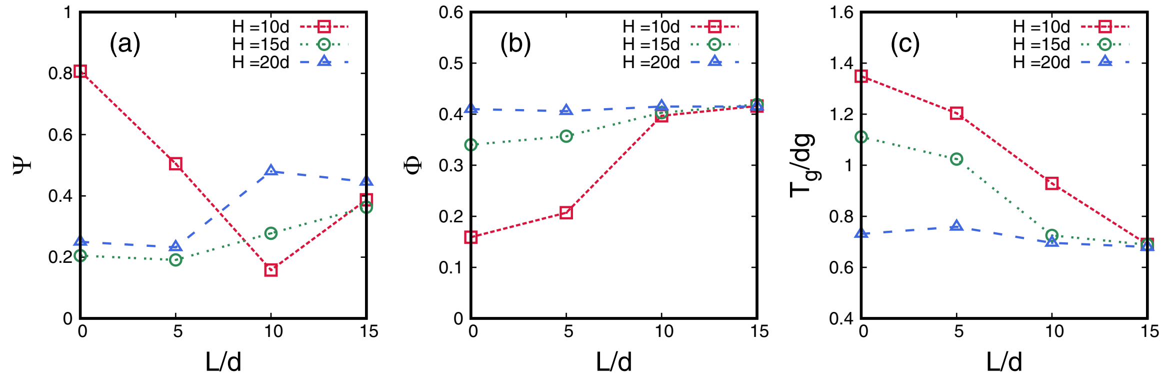

FIG. 9. Variation of (a) clogging index Ψ, (b) packing fraction Φ, and (c) granular temperature T_g for particles in region R with respect to the lateral position L of the obstacle for $W = 11d$ and for three values of H. Here, $D = 22d$.

to flow from left side. The above phenomena coupled with the absence of collisions with particles flowing on the right side results in high horizontal and vertical velocities. This is consistent with the large width on the right side of plot for $L = 5d$ in horizontal velocity distributions. However, for $L \geqslant 10d$, the width of the plot on the right side decreases gradually. As the obstacle is displaced further towards right, most of the particles can reach orifice without detouring around the obstacle. As a result lateral collisions, which are responsible for major variations in velocities, are almost absent for $L \geqslant 10d$ explaining the smaller widths on right side of the plots.

The distribution of the vertical velocity component for different values of L is displayed in Fig. 11(b). The width of the plot is least at $L = 0$, indicating that obstacle hinders the free flow of particles, thus reducing the vertical velocities in region R. Whereas, the widths of plots are slightly broader for $L = 5d$, $10d$ as interference of the obstacle in free flow of particles gradually decreases. However for the case of $L = 15d$, absence of lateral collisions seems to influence both the vertical and horizontal velocity components leading to a decrease in the width of distributions as shown in Fig. 11.

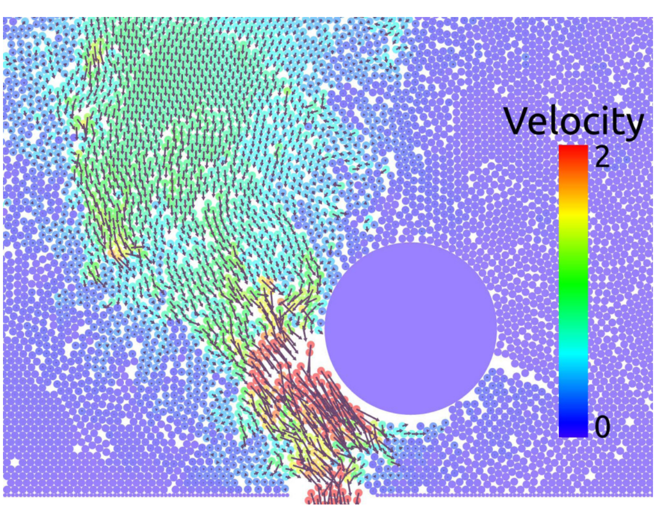

FIG. 10. Velocity magnitude and vector field for the case of $H = 10d$ and $L = 10d$ at a particular instant. The figure also shows the interaction of obstacle with the stagnant zone. The reduction in T_g with L is a consequence of the reduced collision rate due to blocking of the flow on the right.

D. Variation of the obstacle size

Here we consider the effect of varying the obstacle size D (for $L = 0$ and three different values of H) on the clogging index. Figure 12 displays Ψ, Φ, and T_g as a function of D at $W = 11d$ and constant H. Ψ increases with increasing D for $H = 10d$. During the discharge of the particles from the silo a stagnant zone on either side of the orifice is present. As D increases, the distance between the obstacle and stagnant zone(S_d) decreases as shown in Fig. 13. Moreover, the surface exposed to the stagnant zone increases with increase in D. This coupled effect enhances the resistance to the free flow of particles at $H = 10d$ as displayed by high values of Ψ. At $H = 15d$, arches are generally formed involving the obstacle as shown in Fig. 6(b), where S_d should be small enough to form a clog. Though, S_d decreases with increase in D as shown in Fig. 13, at $H = 15d$, its effect is significant only at large diameter of the obstacle, at $D = 44d$ as indicated

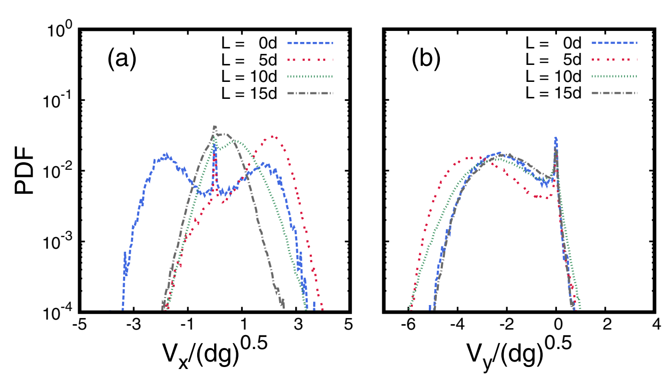

FIG. 11. The probability distribution of the (a) horizontal and (b) vertical velocity component of particles in region R for a silo containing an obstacle with $H = 10d$, $W = 11d$ at various values of L.

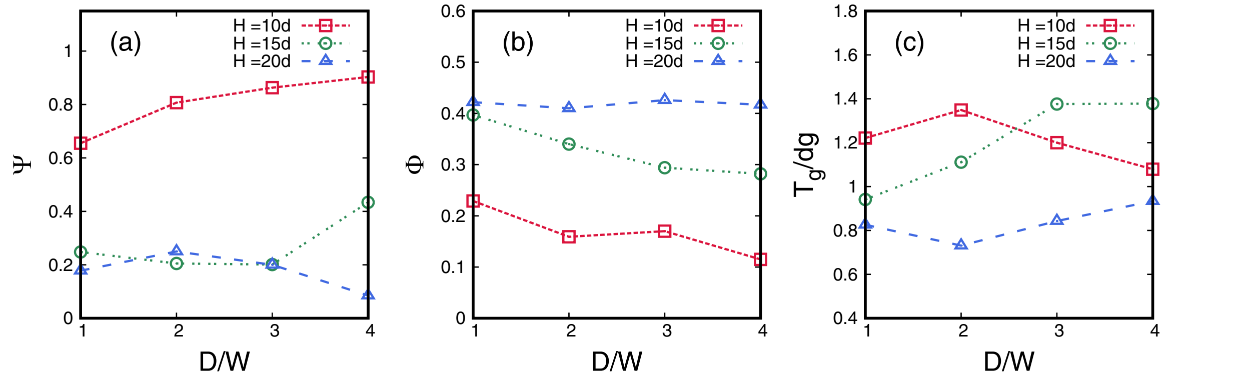

FIG. 12. The variation of (a) clogging index Ψ, (b) packing fraction Φ, and (c) granular temperature T_g with respect to diameter of the obstacle D for various H at $W = 11d$ and $L = 0$.

by the greater clogging probability Ψ. However, at $H = 20d$, Ψ exhibits a nonmonotonic variation with D. This could be attributed to the changes in the orientational dynamics of particles due to the presence of obstacle, which needs to be investigated further. At $H = 20d$, arch formation involving the obstacle is almost negligible as S_d is large. So, the only possibility of arch formation is by particles near the orifice. An increase in D creates a larger wake region below the obstacle, as the particles have to traverse longer path before colliding with particles flowing from opposite side. Thus, Φ decreases with increase in D for $H \leqslant 15d$. However, Φ is almost constant for $H = 20d$ as in this case the wake is formed above region R. T_g increases as D increases for $H \geqslant 15d$ in accordance with the distribution of horizontal velocities in region R for $D \geqslant 22d$ as shown in Fig. 14(a). The distributions of the vertical velocity components are displayed in Fig. 14(b).

IV. CONCLUSION

In the present work, we studied the flow of a monolayer of dumbbells through an orifice at the bottom of a silo. We performed simulations of discharge flow for several orifice widths and observed that the clogging probability is close to zero when the orifice width is greater than $13d$. This is equivalent to 6.5 times the particle length (major dimension of the dumbbell). We also studied the effect of placing an obstacle in the vicinity of the orifice on the granular flow. The size and position of the obstacle have a marked influence on the probability of clogging. While a previous study examined the effect of changing the vertical position only, we also considered changes in the lateral position. Even small displacements away from the vertical axis, can substantially lower the clogging probability.

Compared with spherical particles, the clogging probability of the aspherical dumbbells is markedly higher, though velocity distributions of particles in the vicinity of orifice, which characterize the particle dynamics, are qualitatively similar. It would be interesting to understand the particle dynamics near the orifice for aspherical particles of larger aspect ratios and complex shapes and to investigate whether we can relate their dynamics to the clogging. Another important observation from the present study is the nonmonotonocity of the clogging index as a function of height of the obstacle which is not observed in the case of spherical particles.

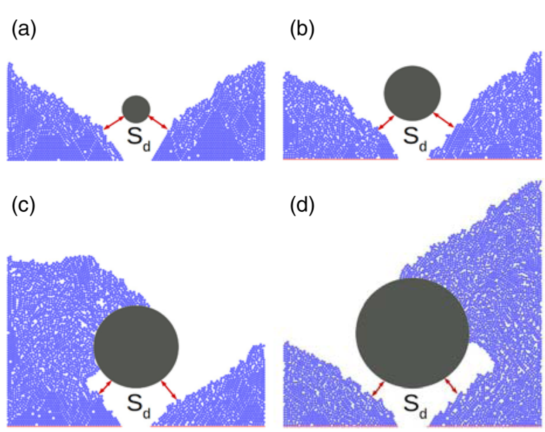

FIG. 13. Representative images showing S_d for (a) D = $11d$, (b) D= $22d$, (c) D= $33d$, and (d) D= $44d$. In all cases, $H = 15d$.

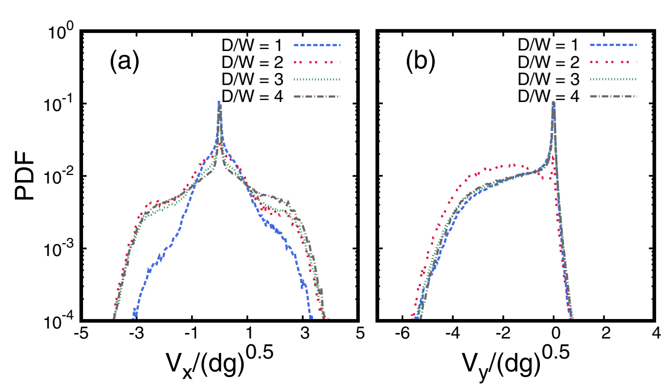

FIG. 14. The probability distribution of (a) velocity component along x and (b) velocity component along y in region R for obstacle position $H = 15d$, $L = 0$ in a silo with an orifice of width $W = 11d$.

[1] A. Garcimartín, J. M. Pastor, L. M. Ferrer, J. J. Ramos, C. Martín-Gómez, and I. Zuriguel, Phys. Rev. E **91**, 022808 (2015).

[2] I. Zuriguel, J. Olivares, J. M. Pastor, C. Martín-Gómez, L. M. Ferrer, J. J. Ramos, and A. Garcimartín, Phys. Rev. E **94**, 032302 (2016).

[3] J. M. Pastor, A. Garcimartín, P. A. Gago, J. P. Peralta, C. Martín-Gómez, L. M. Ferrer, D. Maza, D. R. Parisi, L. A. Pugnaloni, and I. Zuriguel, Phys. Rev. E **92**, 062817 (2015).

[4] D. Helbing, A. Johansson, and H. Z. Al-Abideen, Phys. Rev. E **75**, 046109 (2007).

[5] D. Elliott and D. Smith, Industr. Environ. Crisis Quart. **7**, 205 (1993).

[6] N. R. Johnson, Soc. Probl. **34**, 362 (1987).

[7] B. S. Kerner and H. Rehborn, Phys. Rev. E **53**, R1297 (1996).

[8] Y. Sugiyama, M. Fukui, M. Kikuchi, K. Hasebe, A. Nakayama, K. Nishinari, S. ichi Tadaki, and S. Yukawa, New J. Phys **10**, 033001 (2008).

[9] A. Garcimartín, I. Zuriguel, L. A. Pugnaloni, and A. Janda, Phys. Rev. E **82**, 031306 (2010).

[10] R. C. Hidalgo, C. Lozano, I. Zuriguel, and A. Garcimartín, Granular Matter **15**, 841 (2013).

[11] T. Börzsönyi, E. Somfai, B. Szabó, S. Wegner, P. Mier, G. Rose, and R. Stannarius, New J. Phys **18**, 093017 (2016).

[12] A. Ashour, S. Wegner, T. Trittel, T. Borzsonyi, and R. Stannarius, Soft Matter **13**, 402 (2017).

[13] M. E. Cates, J. P. Wittmer, J.-P. Bouchaud, and P. Claudin, Phys. Rev. Lett. **81**, 1841 (1998).

[14] C. Lozano, G. Lumay, I. Zuriguel, R. C. Hidalgo, and A. Garcimartín, Phys. Rev. Lett. **109**, 068001 (2012).

[15] C. Lozano, I. Zuriguel, and A. Garcimartín, Phys. Rev. E **91**, 062203 (2015).

[16] B. Guerrero, C. Lozano, I. Zuriguel, and A. Garcimartín, EPJ Web Conf. **140**, 03016 (2017).

[17] K. Endo, K. A. Reddy, and H. Katsuragi, Phys. Rev. Fluids **2**, 094302 (2017).

[18] I. Zuriguel, A. Janda, A. Garcimartín, C. Lozano, R. Arévalo, and D. Maza, Phys. Rev. Lett. **107**, 278001 (2011).

[19] C. Lozano, A. Janda, A. Garcimartín, D. Maza, and I. Zuriguel, Phys. Rev. E **86**, 031306 (2012).

[20] F. Alonso-Marroquin, S. I. Azeezullah, S. A. Galindo-Torres, and L. M. Olsen-Kettle, Phys. Rev. E **85**, 020301 (2012).

[21] S. Liu, Z. Zhou, R. Zou, D. Pinson, and A. Yu, Powder Technol. **253**, 70 (2014).

[22] J. Li, P. A. Langston, C. Webb, and T. Dyakowski, Chem. Eng. Sci. **59**, 5917 (2004).

[23] J. F. Favier, M. H. Abbaspour-Fard, and M. Kremmer, J. Eng. Mech. **127**, 971 (2001).

[24] B. Jin, H. Tao, and W. Zhong, Chin. J. Chem. Eng. **18**, 931 (2010).

[25] P. W. Cleary and M. L. Sawley, Appl. Math. Model **26**, 89 (2002).

[26] H. Tao, B. Jin, W. Zhong, X. Wang, B. Ren, Y. Zhang, and R. Xiao, Chem. Eng. Process. **49**, 151 (2010).

[27] P. A. Langston, M. A. Al-Awamleh, F. Y. Fraige, and B. N. Asmar, Chem. Eng. Sci. **59**, 425 (2004).

[28] H. A. Janssen, Z. Ver. Dtsch. Ing. **39**, 1045 (1895).

[29] P. A. Cundall and O. D. L. Strack, Gotechnique **29**, 47 (1979).

[30] N. V. Brilliantov, F. Spahn, J.-M. Hertzsch, and T. Pöschel, Phys. Rev. E **53**, 5382 (1996).

[31] H. P. Zhang and H. A. Makse, Phys. Rev. E **72**, 011301 (2005).

[32] S. Plimpton, J. Comput. Phys. **117**, 1 (1995).

[33] A. Stukowski, Model. Simul. Mater. Sci. Eng. **18**, 015012 (2010).

[34] W. Humphrey, A. Dalke, and K. Schulten, J. Mol. Graph. Model. **14**, 33 (1996).

[35] A. Janda, I. Zuriguel, A. Garcimartín, L. A. Pugnaloni, and D. Maza, Europhys. Lett. **84**, 44002 (2008).

[36] X. Hong, M. Kohne, M. Morrell, H. Wang, and E. R. Weeks, Phys. Rev. E **96**, 062605 (2017).